Int. J. Electrochem. Sci., 5 **(2010)** 1310 - 1341

International Journal of ELECTROCHEMICAL SCIENCE
www.electrochemsci.org

Magnetic Field Effects in Ferrocenealkane Thiol Self Assembled Monolayer Modified Electrodes

Michael E.G. Lyons[*], *Raymond O'Brien, Michael Kinsella, Conchuir Mac Gloinn, P. Noelle Scully*

Physical and Materials Electrochemistry Laboratory, School of Chemistry, University of Dublin, Trinity College, Dublin 2, Ireland.
[*]E-mail: melyons@tcd.ie

Received: 27 July 2010 / *Accepted:* 30 July 2010 / *Published:* 1 September 2010

The redox behaviour of well characterized ferrocene alkane thiol self assembled monolayer modified electrodes in contact with aqueous perchlorate solutions both in the absence of and in the presence of an external magnetic field is examined using both electrochemical and gravimetric techniques The redox switching process has been shown to involve an ET reaction involving the ferrocene/ferricinium redox transition coupled with an ion pairing step involving perchlorate ion. It has been shown that the voltammetric response recorded in the latter medium is irreversibly effected by the imposition of a static magnetic field of magnitude 0.5 T applied in a direction parallel to the electrode surface. Both the surface coverage of electroactive ferrocene surface groups and the electrochemical rate constant for the ferrocene/ferricinium surface redox transformation is quantitatively influenced by the imposition of the external magnetic field. It is suggested that the latter redox transformation is accompanied by ion pair formation between the ferricinium and perchlorate ions . The magnetic field dependence of the redox behaviour can be attributed to structural changes in the monolayer arising from double layer effects involving changes in the spatial distribution of perchlorate counterions at the monolayer/solution interface, the latter brought about by local convective stirring arising from the B field generated magnetohydrodynamic Lorenz body force.

Keywords: ferroceneyl alkane thiol self assembled monolayer, chemically modified electrodes, magnetoelectrochemistry, redox active monolayers.

1. INTRODUCTION

The technology for the assembly of single molecules and other nanoscale components into robust and reproducible two and three terminal electronic devices is still in its infancy. Thorough and

quantitative studies of electron transfer in single molecule device structures remains extremely challenging [1]. On the other hand, redox active molecules tethered to ordered self assembled organic nanostructures of monolayer thickness immobilized on metal electrodes provide a well defined and versatile way to probe the mechanism of molecular electron transfer and tunnelling through organic materials [2]. Mixed monolayer systems containing both redox active and analogous electroinactive structures which serve as diluents can be readily prepared, and so the surface confined redox species can be diluted in a controlled manner to generate an array in which the redox sites are far enough apart so that they do not interact with one another. The application of well established electrochemical techniques to the latter system offers the ability to answer many thermodynamic, kinetic and structural questions relevant to the construction of molecular electronic devices.

Magnetic field effects on electrochemical reactions have been recently reviewed [3] and may be divided into three categories-those relating to mass transport, deposit morphology and electrode kinetics. The effect of a magnetic field on mass transport is well established. The field acts to induce convection in the solution, thereby reducing the diffusion layer thickness and thus increasing the diffusion limited current [4]. In recent years, clear field effects on the morphology and texture of electrodeposits have been reported under various conditions [5].

The effect of external magnetic fields on the dynamics of heterogeneous electron transfer processes is more controversial. Some authors report that the field has no influence [6] whereas others explain modifications in the exchange current density in a field in terms of transitions between magnetic quantum states in the ions [7].

In this communication we report the marked effect of an external static magnetic field (0.5 T) on the redox and electron transfer behaviour of a self assembled redox active monolayer (SAM) n-(ferrocenylcarbonyloxy) alkane thiol $FcCO_2(CH_2)_nSH$, when n = 7,10,11,12. Here the ferrocene/ferricinium redox couple is immobilized in a well defined surface nanostructure and is not free to diffuse in solution. As such one might expect that the redox couple should not itself exhibit any mass transport based Lorenz magnetohydrodynamic force. However we will show that the magnetic field effects the environment surrounding the tethered redox moeity and in particular effects the counterion distribution adjacent to the SAM.

2. EXPERIMENTAL

2.1 Chemicals

Hexane-, octane-, decane-, undecane- and dodecane-thiol (98+%, Aldrich), perchloric acid (70%, Merck) and ethanol were used as received.Thiourea (99%), potassium hydroxide, (2-Chlorobenzoyl) Chloride, N, N'- dicyclohexylcabodiimide (DCC), 4-(dimethylamino)pyridine (DMAP), sodium hydride (95%) and 12-bromo-1-dodecanol were purchased from Sigma-Aldrich.

Dichloromethane and dimethylether (DME) were distilled over calcium hydroxide. Water for preparing electrolyte solutions and rinsing of electrodes was purified using a Millipore MilliQ system (water resistance 18 MΩ).

2.2. Synthetic procedure

A series of n-ferrocenylcarbonyloxyalkanethiols $FcCO_2(CH_2)_nSH$ (n = 6, 8, 10,11 and 12) were synthesised using literature procedures [8,9]. A two step synthetic strategy was adopted. The first step involved the synthesis of the pertinent n-(Ferrocenylcarbonyloxy)alkyl Bromide moeity, via esterification of ferrocene carboxylic acid and the desired n-bromoalcohol in a Mitsunobu coupling reaction. N, N'- dicyclohexylcabodiimide (DCC) was used as a coupling reagent and the reaction was catalysed by 4-(dimethylamino)pyridine (DMAP), producing the desired product in ~50% yield and dicyclohexylurea (DCU) as a by-product. By varying the chainlength of the bromo-alcohol in this reaction, the corresponding chainlength alkyl halide product is obtained. In the second stage, the pertinent alkyl bromide was refluxed with thiourea in absolute ethanol, causing the nucleophilic displacement of the alkyl halide and the formation of an isothiuronium salt. The thiol was then generated by base hydrolysis of the isothiuronium salt. The thiols were obtained as light brown solids in ~50% yield. The final products were characterized by ESMS, IR and ^{1}H NMR.

A detailed description of the 12-ferrocenylcarbonyloxyalkanethiol $FcCO_2(CH_2)_{12}SH$ moiety is provided here. Full synthetic details of other alkane thiol materials follow similar protocols and have been described by MacGloinn [8]. The synthetic methodology is outlined in scheme 1.

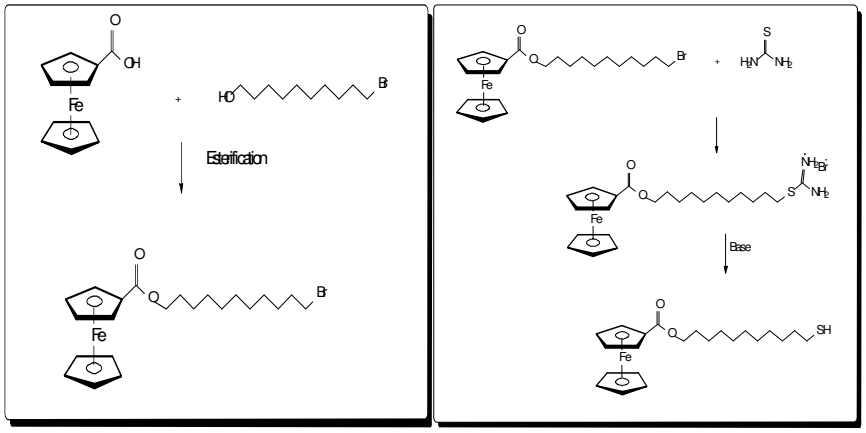

Scheme 1. Outline of alkane thiol synthetic methodology

2.2.1. Preparation of (2-Chlorobenzoyl) Ferrocene [10]

A thoroughly dried, three-necked, round-bottomed flask (500ml) was charged under nitrogen with Ferrocene (9.3g, 0.05mol), (2-Chlorobenzoyl) Chloride (6.33ml, 0.05mol) and dry DCM (100ml), forming an orange solution. Anhydrous Aluminum Chloride (6.67g, 0.05mol) was slowly added over a period of fifteen minutes, while the reaction mixture was kept below 5°C. The mixture was stirred with cooling for a further 30 minutes and then for another 2 hours at room temperature, by which time the reaction mixture had turned a deep blue. The reaction mixture was once again cooled and water (100ml) was cautiously added. The resulting two-phase mixture was vigorously stirred for a further 30 minutes. The layers were then extracted using DCM (2 x 30ml). The combined extracts were then

washed with water (50ml) and 10% NaOH (2 x 50ml), before being dried over magnesium sulphate. After filtration and evaporation to dryness at reduced pressure, the product was found to be a red crystalline substance (15.3g, 94.3% yield).

^{1}H NMR (400Hz, $CDCl_3$): δ 4.28ppm (s, Cp, 5H), 4.6ppm (aps, 2(CHCHCCO), 2H), 4.76ppm (aps, CHCCO, 2H), 7.36-7.54ppm (m, Ar, 4H).
ESMS (MeCN): $C_{17}H_{13}OCl(M^+)$ requires: 325, found 325.

2.2.2. Preparation of Ferrocene Carboxylic Acid [10]

Potassium tertiary butoxide (13.46g, 0.12mol) was dissolved in dry DME (150ml) and left to stir under nitrogen for 10 minutes. Water (0.657ml, 0.0365mol) was added to the reaction mixture, producing a white slurry. (2-Chlorobenzoyl) Ferrocene (11.85g, 0.0365mol) was added and the reaction mixture was refluxed for 1 hour. The reaction was accompanied by a colour change from red to tan. The reaction mixture was then cooled and poured into water (500ml). The resulting solution was then washed with diethyl ether (3 x 75ml) and back-extracted with 10% NaOH (2 x 50ml). The aqueous phases were combined, acidified with concentrated HCl, and the resulting precipitate was collected by filtration. The required product was air dried to yield a yellow powder (6.85g, 81.6%).

^{1}H NMR (400Hz, $CDCl_3$): δ 4.28 (s, Cp, 5H), 4.49 (aps, 2(CHCHCCO), 2H), 4.88ppm (aps, CHCCO, 2H).
^{13}C NMR (400Hz, $CDCl_3$): δ 70.1 (Cp), 70.6 (2 x CHCHCCO), 72.0 (2 x CHCCO), 177.1ppm (C=O).
ESMS (MeCN): $C_{11}H_{10}O_2(M^+)$ requires: 231, found 231.

2.2.3. Preparation of 12-(Ferrocenylcarbonyloxy)dodecyl Bromide n=12

A thoroughly dry Schlenk tube was equipped with a mechanical stirrer and a stopper. The reaction vessel was evacuated of air and a N_2 atmosphere was established. Ferrocene Carboxylic Acid (0.9541g, 4.15mmol), 12-Bromo-1-dodecanol (1g, 3.7mmol) and DMAP (50.7mg, 0.415mmol) were placed in the tube. The tube was stoppered and dry DCM (25ml) was injected under N_2 into the system. The dark yellow reaction mixture was then cooled to 0°C and DCC (0.9335g, 4.52mmol) was added. The reaction was left to stir for 1 hour at 0°C and stirred overnight at RT. After removal of the precipitated dicyclohexylurea (DCU) by filtration, the product was recovered by extraction with DCM. The DCM extracts were then washed with dilute HCl (2 x 25ml), water (2 x 25ml), dried over magnesium sulphate, filtered and evaporated under reduced pressure. The product was dissolved in DCM and chromatographed on silica with DCM. The first yellow band contained the required product which was isolated by TLC and evaporated to dryness (a light brown solid, 0.867g, 49.3%).

^{1}H NMR (400Hz, $CDCl_3$): δ 1.31-1.44ppm (broad, 16H), 1.72ppm (t, J= 6.83 Hz, 2H), 1.85ppm (t, J= 6.83 Hz, 2H), 3.41ppm (t, J= 6.83 Hz, 2H), 4.22ppm (s, 7H), 4.41ppm (s, 2H), 4.83ppm (s, 2H).

ESMS (MeCN): $C_{23}H_{33}0_2Br(M^+)$ requires: 477, found 477.

2.2.4. Preparation of 12-(Ferrocenylcarbonyloxy)dodecyl Thiol n=12

A thoroughly dry Schlenk tube was equipped with a mechanical stirrer and a stopper. The reaction vessel was evacuated of air and a N_2 atmosphere was established. 12-(Ferrocenylcarbonyloxy)dodecyl bromide (0.551g, 1.15mmol) and thiourea (0.263g, 3.45mmol) were added to absolute ethanol (25ml), and the resulting solution was stirred and refluxed under N_2 overnight. The solvent was then removed under vacuum and an aqueous solution of potassium hydroxide (25ml, 0.193g, 3.45mmol) was added, and then the mixture was refluxed for 4 hours under N_2 and then cooled to room temperature. The resulting solution was extracted with DCM (3 x 50ml) and the combined extract was washed with dilute HCl (2 x 50ml) and water (2 x 50ml). The extract was dried over magnesium sulphate, filtered, concentrated under reduced pressure and chromatographed on silica with DCM. The first yellow band contained the required product (a brown solid, 0.26g, 52% yield).

FTIR: 1274 (C-O), 1710 (C=O), 2570 (S-H)
^{1}H NMR (400Hz, $CDCL_3$): δ 1.3 - 1.44ppm (broad, 17H), 1.58ppm (m, 2H), 1.71ppm (m, 2H), 2.51ppm (q, J= 7.51Hz, 2H), 4.25ppm (s, 7H), 4.43ppm (s, 2H), 4.85ppm (s, 2H).
ESMS (DCM): $C_{23}H_{34}O_2S(M^+)$ requires: 430, found 430.

2.3. Electrodes and cells

Gold macroelectrodes supplied by IJ Cambria with a substrate area of 0.0314cm^2 were used to carry out electrochemical measurements that did not require EQCM data. Experiments requiring EQCM were carried out on a gold working electrode with an area of 0.196cm^2. An Ag/AgCl reference electrode supplied by IJ Cambria was used in this report. The electrode was stored in a 3M solution of KCl when not in use. In this work a platinum wire supplied by IJ Cambria was used as the counter electrode.

A CH Instruments Model 440 Electrochemical Quartz Crystal Microbalance was used to gather all electrochemical EQCM data. The system contains a quartz crystal oscillator, fast digital function generator, high speed data acquisition circuitry, a potentiostat and a galvanostat. The potential control range of the instrument is ±10V and the current range is ±250mA. Data was processed using an Advent 3036A Model W0311 Pentium 3 processor PC. All other routine electrochemical measurements were performed using a BAS 100W Electrochemical workstation controlled by a Dell Optiplex PC. Electrochemical measurements were carried out using a standard three electrode electrochemical cell.

The electrochemical quartz crystal microbalance is a variant of acoustic wave microsensors that are capable of ultrasensitive mass measurements. Under favourable conditions a typical EQCM can measure a mass change of 0.1-1ng/cm^2. The QCM technique was first identified by Sauerbrey [9]. QCM oscillates in a mechanically resonant shear mode under the influence of a high frequency AC

electric field applied across the thickness of a quartz crystal. The top and bottom sides of the quartz crystal are coated with a layer of gold that act as the working electrode.

The mass sensitivity of EQCM originates from the relationship between the oscillation frequency of the total mass of the crystal and the oscillation frequency of the crystal with adlayers of material residing on the metal coated crystal. This relationship is shown in Eqn.1 and is known as the Sauerbrey Equation [11]:

$$\Delta f = -\frac{2 f_0^{\,2}}{A\sqrt{\mu\rho}}\Delta m \qquad (1)$$

Here f_0 is the resonant frequency fundamental to the crystal , A is the area of the gold electrode coated onto the crystal, ρ is the density of the crystal and μ is the shear modulus of quartz. In the CH Instruments Model 440 system these values are, f_0 = 8MHz, A = 0.196cm^2, ρ = 2.648g.cm^{-3}, μ = 2.947 x 10^{11} g.cm^{-1}.s^{-2}. Using these values it is seen that a frequency change of 1Hz corresponds to a mass change of 14ng using the CH Instruments Model 440 EQCM. The minus sign in eqn.1 determines that a frequency decrease corresponds to a mass increase.

The EQCM cell consisted of three cylinderical Teflon sections. The total height of the cell was 37mm and its diameter was 35mm. The top section is the cell top that holds the counter and reference electrodes. There are also two 2mm holes which facilitate solution degassing via nitrogen purging. The centre section is the cell body used for holding the solution. The bottom section is used for mounting the quartz crystals. Four screws are used to seal the bottom and centre pieces together. The quartz crystal was located between the bottom and centre sections. The top section may be pressed into the centre section to complete the cell.

In this work the surface of gold macroelectrodes were renewed by carrying out a standard polishing procedure prior to experiments to produce a reproducible surface morphology and freedom from adsorbed impurities as verified by analysis using cyclic voltammetry (CV). The polishing kit used in this surface renewal process contained a range of alumina polishing powders and a range of polishing pads composed of different material. The polishing powders used were: 1.0 micron Alpha alumina powder, 0.3 micron Alpha alumina powder and 0.05 micron Alpha alumina powder. Three polishing pads were used. These were composed of: 1200 grit Carbimet disks, Nylon and Microcloth. All pads were discs and were 73mm in diameter. In order to polish the gold macroelectrodes they were first rotated in a figure of eight motion on bare Carbimet pads for 1 minute in order to remove any visible scratches if they existed. Such scratches were rare and normally occurred only if an electrode was accidentally dropped. If no scratches were visible this polishing stage was not carried out. Following this the electrodes were polished in a figure of eight motion for one minute on the Nylon polishing pads covered with a paste made from 1.0 micron alumina powder and Milllipore water. The electrodes were then thoroughly rinsed with Millipore water and transferred to a separate Nylon polishing pad covered with a paste made from 0.3 micron alumina powder and Milllipore water. Again they a figure of eight motion for 1 minute was used for polishing. The electrodes were again thoroughly rinsed in Millipore water. Finally the electrodes were transferred to a Microcloth polishing

pad covered with a paste made from 0.05 micron alumina powder and Milllipore water. Again a figure of eight motion for 1 minute was used for polishing. This completed the electrode surface renewal. Normally the electrodes were rinsed again with Millipore before being inserted into the electrochemical cell.

Due to the nature of the EQCM gold electrodes it was not possible to use this polishing step. The EQCM electrodes are delicate and only a thin film of gold is deposited on the surface. Any polishing step would certainly have stripped the gold layer from the crystal. The EQCM crystals were instead placed in 3.6% HCl for 5 minutes then rinsed with copious amounts of millipore water and finally rinsed with copious amounts of the solvent chosen to deposit the monolayer. This approach yielded reproducible surface morphology as verified by CV.

Alkane thiol self assembled monolayers were formed on gold support electrode surfaces via a solution adsorption technique. Firstly the electrodes were rinsed with copious amounts of the solvent of choice. The gold electrodes were then immersed, at open circuit, in a 1mM solution of alkanethiol in a selected organic solvent for a period of 48 hours. Upon removal from the thiol solution the electrodes were again rinsed with copious amounts of solvent to remove any physisorbed species. Thiols were prepared using ethanol, methanol, hexane, toluene and acetonitrile. The most common solvent used was ethanol due to its faint odour, low toxicity and ready availability. It was found that the initial solution adsorption process was relatively rapid and the subsequent self assembly process occurred over a considerably longer timescale. The n-mercapto ferrocenecarboxylate alkane thiol moiety is converted upon adsorption to the n-sulfidoferrocenecarboxylate alkane thiolate due to the loss of the mercapto hydrogen and the formation of a gold thiolate bond.

2.4. Generation of Uniform magnetic fields

The performance of electrochemical measurements in a well defined external magnetic field environment is not trivial. Firstly one must ensure that the electrochemical cell can be placed within the magnetic field and second, the magnetic field must be uniform and exhibit a minimal field gradient. Static magnetic fields may be produced by either a steady electric current or a permanent magnet.

The conventional method by which a magnetic field is produced is to pass a current through a solenoid. From basic physics we can readily show that the magnetic field strength **H** (units: Am^{-1}) depends on the product of the current I and the number of turns per unit length of the coil n: $\mathbf{H} = nI$. The magnetic field strength is therefore easily varied. The field can be amplified and directed by winding the solenoid on a ferromagnetic iron yoke with an air-gap. This is the basis of the solenoidal electromagnet, which can be used to generate fields up to about 1600 kAm^{-1}. However in a solenoid with electrical resistance R, energy will be dissipated as heat at a rate proportional to I^2R. Of course if the heat is not removed, the resistance of the coils will increase, thereby reducing the current and hence the magnetic field. Heat removal requires a cooling system which can prove expensive, and for increasingly large fields the DC current, solenoid size and cooling system must be scaled correspondingly. Furthermore maintenance of the field requires a continuous expenditure of energy

and if the field strength is critical an expensive current control device will also be required. If it is essential that the field created be homogeneous (as is the case in electrochemical work) then a further constraint is placed on the design leading to a greater complexity and cost. An alternative approach (especially for the generation of fields greater than 1600 kA m^{-1}) is to use non-resistive superconducting solenoids. Using modern superconducting materials it is possible to generate fields of 10^7 A m^{-1}.

In an environment where there is no source of electric power or cooling water or if there are constraints on the device dimensions, permanent magnets offer a clear advantage over electromagnets. Permanent magnet devices generally consist of a number of other components besides the magnetic material. These may include soft ferromagnetic materials used to guide and concentrate the magnetic flux into the working area. The entire assembly of magnets, soft iron and air gap is termed a magnetic circuit. The two major rare earth permanent magnets (REPM) are Samarium-Cobalt ($SmCo_5$ and Sm_2Co_{17}) and the more recently developed Neodynium-Iron-Boron ($Nd_2Fe_{14}B$). These materials afford the possibility of the generation of homogeneous magnetic fields of high intensity in a permanent magnet structure. Also the high energy density exhibited by these materials (values in excess of 400 kJ m^{-3} have been observed for $Nd_2Fe_{14}B$) means that permanent magnets made from such materials have smaller volumes than those made with conventional magnetic materials.

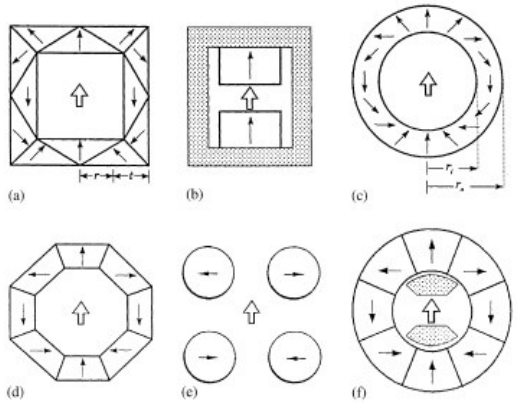

Figure 1. Permanent magnet structures which generate transverse uniform magnetic fields in the air gap region .

Permanent magnets are unique in their ability to deliver magnetic flux into the air gap of a magnetic circuit without any continuous expenditure of energy. By assembling long cylindrical magnet segments around a hollow bore it is possible to create a field which is uniform within a certain region of space and zero elsewhere. Choosing the orientation of each segment appropriately, the fields will all add at the centre. The flux density is the airgap B(r) scales with, but is not limited by the remant polarization B_r of the magnetic material. Hence $B(r) = K(r) B_r(r)$, where K(r) denotes the geometric constant of the magnetic circuit. When K > 1 the circuit achieves flux concentration. A cross section of some permanent structures which generate a uniform magnetic field in the direction shown by the

hollow arrow are presented in figure 1. Options c and d are those most suitable for electrochemical studies.

In figure 1(c) a design is outlined in which the direction of magnetization of any segment is at an angle $\alpha = 2\theta$ from the vertical axis. Here all segments will contribute to create a uniform field across the air gap in the vertical direction. Unlike the configuration presented in figure 1(a) , the radii r_1 and r_2 can take any values without creating a stray field outside the cylinder. This configuration is commonly called a Halbach cylinder. The flux density in the air gap of an ideal infinitely long cylinder is given by $B = B_r \ln\left(r_2/r_1\right)$ where r_1 and r_2 are the inner and outer radii of the cylinder. In practice is not feasible at present to make a cylinder from a single piece of material in which the magnetization angle α changes continuously, and so it is convenient to assemble the device from n trapezoidal segments as illustrated in figure 1(d) for n = 8. In this case the field at the centre of the air gap by a finite cylinder of n trapezoidal segments is:

$$B = B_r \ln\left(\frac{r_2}{r_1}\right)\left\{\frac{\sin\left[2\pi/n\right]}{2\pi/n}\right\} \cong B_r \ln\left(\frac{r_2}{r_1}\right)\left\{\frac{\cos\left[\pi/n\right]\sin\left[\pi/n\right]}{\pi/n}\right\} \qquad (1)$$

where the approximation on the right hand side of the latter expression becomes better as n -> ∞. Note that an eight segment cylinder given 90% of the field of an ideal cylinder. We note that small values of n, of the order eight, twelve or sixteen segments are optimal however in practice since increasing complexity and cost associated with increasing n is not justified by the marginal increase in field obtained. As noted in figure 1 the individual segments can exhibit a variety of shapes but the important criterion for maintenance of field homogeneity is that the centres of the segments lie on a circle. Furthermore, for an infinitely long cylinder the field B_∞ is constant along the central axis. In the case of a cylinder of finite length L there are two effects to be noted. Firstly, the field B_L will be less than B_∞ . Secondly, the field homogeneity along the cylindrical axis will be reduced. The reduction in flux density at the center can be expressed in terms of a field reduction factor F given by: $F = \frac{B_\infty - B_L}{B_\infty} = 1 - \frac{B_L}{B_\infty}$. We can show that the magnetic flux at the centre of a cylinder of finite length L is given by:

$$B_L = \frac{B_r}{2}\left\{2\ln\left(\frac{r_2}{r_1}\right) + \frac{1}{\sqrt{1+\left(2r_1/L\right)^2}} - \frac{1}{\sqrt{1+\left(2r_2/L\right)^2}} - 2\ln\left\{\frac{1+\sqrt{1+\left(2r_2/L\right)^2}}{1+\sqrt{1+\left(2r_1/L\right)^2}}\right\}\right\} \qquad (2)$$

and for the infinite length cylinder $B_\infty = B_r \ln\left(r_2/r_1\right)$. Hence F may be calculated for various ratios of r_2/r_1 and as a function of cylinder length L . Note that a cylinder made of 8 trapezoidal segements with dimensional ratios $r_2/r_1 = 1.7$ and $L/2r_1 = 2.5$ made from a metarial with remanence

B_r = 1.2 T will produce a central field B of ca. 0.6 T. In our electrochemical work we have found that long permanent magnet cylinders known as Halbach cylinders or dipole rings with dimensions similar to those just quoted create a magnetic field in their bore which, to a good approximation, is uniform . The computed flux distribution within a Halbach cylinder is illustrated in figure 2 [12]. Also, two such cylinders can be coaxially nested and rotated about their common axis to create a variable magnetic field.

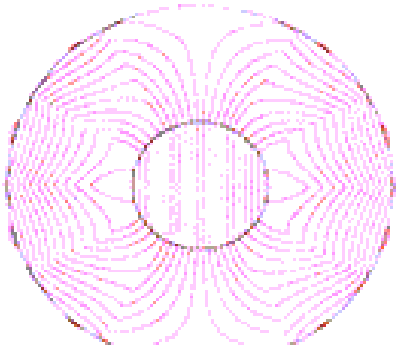

Figure 2. Magnetic flux lines calculated for Halbach cylinder of the type used in the present work.

Two different sources of magnetic field were employed in this work. The first was a Magnetic Solutions HC-500-54 Hallbach cylinder which was constructed from $Nd_2Fe_{14}B$ and generated a fixed static field of 0.5 T transverse to the bore which was 54 mm diameter. The second was a Magnetic solutions MM-1000-48 Multimag. The latter system consisted of two nested Hallbach cylinders which could be rotated relative to one another by stepper motors to produce a variable static magnetic field in the range 0 – 1 T. In this case the bore diameter was 48 mm.

Photographs of the experimental setup employed using the Multimag system are presented in figure 3. The magnetic field is applied to the working electrode by placing the entire electrochemical glass cell in the bore of the Halbach magnet. Since the working electrodes usually consist of discs inlaid in glass the latter arrangement ensures that the lines of magnetic flux density are oriented parallel to the surface of the working electrode. The latter arrangement was used in all variable magnetic field studies described in this paper.

Macroelectrode experiments involving the magnetic field involved firstly coating the electrode with a SAM from a dilute solution of thiol. Cyclic voltammetry was then performed in the absence of a magnetic field to ensure monolayer quality. The electrochemical cell was then placed in the bore of the magnet with the direction of the magnetic field running parallel to the surface of the working electrode and hence perpendicular to the direction of the alkane chains on the surface of the monolayer. Cyclic voltammograms were then run continuously between the upper and lower voltage

limits and scans performed after defined time intervals in the bore of the magnet were selected for analysis. Certain experiments involved analysis of the SAM redox activity when the field was removed. In this case the electrochemical cell was removed from the bore of the magnet after analysis and subsequent cyclic voltammetry was performed in the absence of the magnetic field

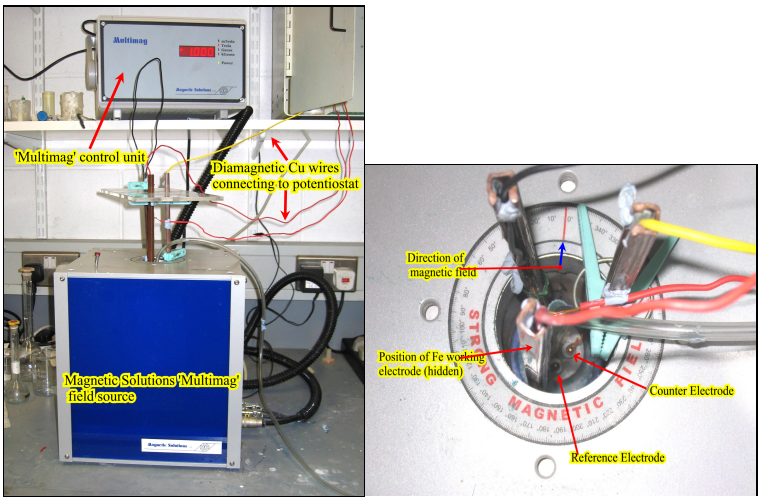

Figure 3. Variable magnetic field Hallbach based Multimag System (Magnetic Solutions Ltd) setup for electrochemistry experiments. The custom built electrochemical cell is located within the bore of the cylindrical magnet.

During EQCM experiments the entire Teflon cell was carefully placed into the bore. Because of the design of the EQCM cell little could be done to ensure that the orientation of the B-field relative to the electrodes was exactly the same during different experiments. However the technique for voltammetric analysis in the presence of the magnetic field was identical to that used in the case of macroelectrodes.

3. RESULTS AND DISCUSSION

3.1. Effect of external magnetic field on cyclic voltammetric response of monolayer immobilized ferrocene/ferricinium redox couple

In figure 4 we show the voltammetric behaviour recorded in 0.1 M $HClO_4$ solution at a sweep rate of 20 mVs^{-1} for the 12-ferrocenylcarbonyloxyalkanethiols $FcCO_2(CH_2)_{12}SH$ SAM film assembled on a polycrystalline gold support electrode, in the absence and in the presence of an external magnetic field (B = 0.5 T). This experiment was performed in an electrochemical cell placed directly in the bore of a Hallbach magnet in which the direction of the constant and uniform magnetic field (B = 0.5 T) was set parallel to the surface of the working electrode. A well defined pair of redox peaks corresponding to the ferocene/ferricinium surface redox transition are clearly discerned with E^0 having

a value close to 582 mV (vs Ag/AgCl) at slow sweep rates. The latter does not change when an external magnetic field is applied, hence the thermodynamics of the surface redox transformation (as defined by the E^0 value) is not field dependent.

It is well established that the surface coverage of the redox active surface group may be calculated via analysis of the integrated charge associated with either the anodic or cathodic voltammetric peak using the relation: $\Gamma = Q_{CV}/nFA$ [13] . Since n = 1 for the Fc/Fc^+ couple we can immediately calculate the surface coverage.

It is immediately obvious from fig.4 that a marked decrease in surface coverage of attached electroactive ferrocene species was observed in the presence of the magnetic field ($\Gamma = 0.79$ nmol cm^{-2} (B = 0T) and $\Gamma = 0.52$ nmol cm^{-2} (B = 0.5T)). Hence $\Gamma_B/\Gamma_0 = 0.60$. This decrease in surface coverage was irreversible. When the redox active monolayer modified electrode was again subjected to a potential cycling experiment in the absence of a magnetic field the profile did not recover and the observed current intensity did not revert to its value observed before the monolayer was scanned in a magnetic field.

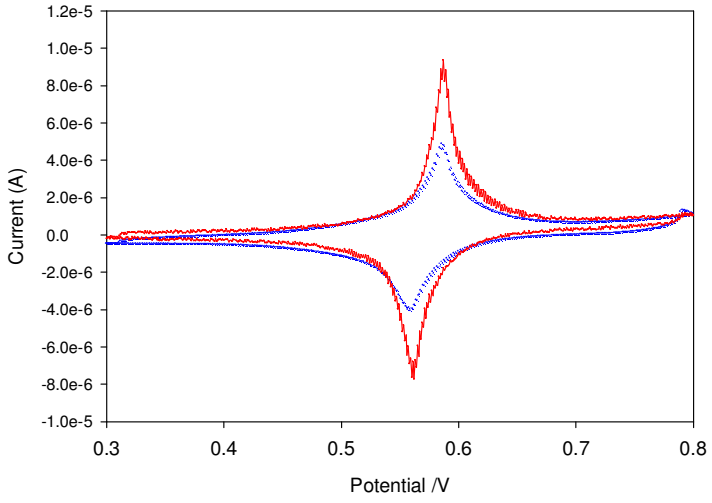

Figure 4. Cyclic voltammetric response for the ferrocene thiol $FcCO_2(CH_2)_{12}SH$ SAM recorded both in the presence (blue trace) and in the absence (red trace) of an external magnetic field of magnitude 0.5 T, Electrolyte 0.1 M $HClO_4$, sweep rate 20 mV/s.

This is a very unusual observation, and to the best of the authors knowledge has not been reported before in the literature. An immediate inference might be that the ferrocene/ferricinium moiety is unstable in aqueous $HClO_4$ media. However the latter assertion is at variance with the many experiments conducted in our laboratory. The first noteworthy point derived from the latter work is that stable cyclic voltammograms are obtained on repetitive potential cycling over an extended potential range in aqueous perchlorate solutions ($HClO_4$ and $NaClO_4$). We have also shown that the shapes of the voltammograms recorded in each electrolyte solution are distinctive, and are

characteristic of the electrolyte. The observation of layer stability in ClO_4^- containing electrolytes in accordance with previous literature observations [14].

It has been established [15,16] for example that ferricenium $FeCp_2^+$ decomposes through exchange of a cyclopentadienyl ligand with another nucleophile, especially OH^- and Cl^- and NO_3^-. The rate of exchange increases with the donor strength of the nucleophile. The Cp^- species can then reduce un-dissociated $FeCp_2^+$ to $FeCp_2$ in a follow up reaction. As a result cyclopentadienyl radicals are

formed which are lost through irreversible combination or hydrogen abstraction reactions. It has been shown that ferrocene derivatives follow a similar decomposition pathway, although the rate of the latter is dependent on the electron withdrawing/donating strengths of the substituents. It is not unreasonable that the surface immobilized analogue should also exhibit a similar reactivity pattern [15,16]. Porter and co-workers [14] have examined the stability in 1 M $HClO_4$ of ferrocene terminated monolayers formed on gold electrodes by the chemisorption of 11-mercaptoundecyl ferrocenecarboxylate $FcCOO(CH_2)_{11}SH$ using a combination of cyclic voltammetry and in situ infrared reflection-absorption spectroscopy (IRRAS). These workers found that the half life of the immobilized ferrocene unit follows the donor strength found in the previous solution phase studies where $Cl^- > Br^-$, $>NO_3^- > SO_4^{2-}$.

Porter et al therefore suggested that there was a mechanistic transition in the decomposition chemistry from the solution phase to the surface bound phase. In our own independent studies [8,9b,17] we have noted that repetitive potential cycling in HCl and KCl solution causes rapid deterioration of the monolayer film as evidenced by the progressive decrease in anodic and cathodic peak intensities and integrated peak charges on repetitive potential cycling in the latter media. It is important to note that the loss of peak intensity is due to the loss of the ferrocenyl moiety and can not be attributed to the desorptive loss of the layer arising from cleavage of the Au-S bond.

Porter and co-workers [14] found that in 1 M $HClO_4$, loss of ferrocene coverage is minimal provided that the redox centre is kept predominantly in the reduced Fc form. Significant (> 50%) loss occurs over hours if the redox sites are held in the oxidized ferricinium form whether in ! M $HClO_4$ or 0.1 M $NaClO_4$.

The experiment was repeated for a series of ferrocene alkane thiol SAM modified electrodes of varying hydrocarbon chain length, and as a typical example, the result for the $FcCO_2(CH_2)_7SH$ SAM is illustrated in fig.5 where a similar decrease in surface coverage is observed when the film is cycled in a B field of 0.5 T. Typically for all alkanethiol films examined, $\Gamma_B/\Gamma_0 \cong 0.5-0.8$, and indeed the observed ratio was variable due to the inherent irreproducibility of fabricating alkane thiol SAMs on gold surfaces via the passive (open circuit) incubation method adopted.

Chidsey [18] calculated that the maximum coverage of surface immobilized ferrocene alkanethiol molecules should be 0.45 nmol cm^{-2} assuming a close packed layer of 6.6 angstroms diameter spheres. The experimental coverage values measured under zero external field conditions, are somewhat larger and probably reflect an uncertainty in the true surface area and the presence of some structural disorder in the SAM film. The latter disorder prevents all the attached ferrocene units from lying in the same plane. The coverage values obtained in the presence of the magnetic field are closer in magnitude to the ideal figure of merit calculated by Chidsey [18] and may well reflect a decrease in structural disorder in the SAM layer when the field is applied.

The observation that this decrease in measured surface coverage is irreversible would tend to support the latter contention since the monolayer would not be expected to revert to a more disordered form when subjected to a potential cycling programme in the absence of an external magnetic field.

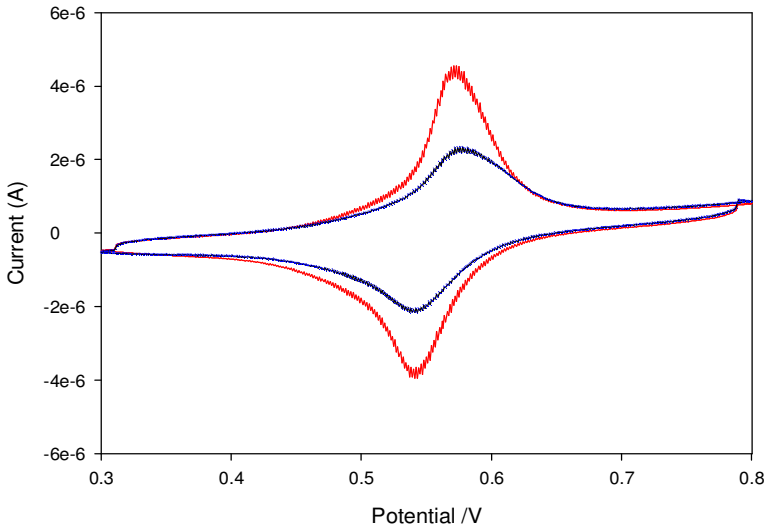

Figure 5. Cyclic voltammetric response for the ferrocene thiol $FcCO_2(CH_2)_7SH$ SAM recorded both in the presence (blue trace) and in the absence (red trace) of an external magnetic field of magnitude 0.5 T, Electrolyte 0.1 M $HClO_4$, sweep rate 20 mV/s.

It is still unclear whether the deposition solvent can affect the properties (especially the degree of ordering) of alkane thiol SAM films. It has been noted that poor solvents may increase the driving force for adsorption of the thiol from solution onto the substrate surface. However a long alkane chain may exhibit significant coiling in a poor solvent so that the stretching and close packing of the alkane chain requires a longer time period. In contrast hexadecane and other long chain hydrocarbon solvents are suspected of inducing disorder in the SAM because of the tendency of these solvents to intercalate into the organized monolayer.

We therefore conducted a series of experiments to establish whether a magnetic field effect would be seen in ferrocene alkane thiol SAM films formed via passive deposition from different organic solvents such as acetonitrile, hexane, toluene and ethanol. The results of this work are presented in fig.6 where the voltammetric response of ferrocene alkane thiolate SAM films formed on gold substrates via passive deposition from a 1 mM solution of $FcCO_2(CH_2)_{10}SH$, in four different solvents in the absence and presence of a 0.5 T B field are illustrated. The sweep rate used in each case was 100 mV/s and the electrolyte solution was 0.1 M $HClO_4$. We note that the reduction in redox peak intensity on scanning in a finite B field is greatest for SAM films formed from ethanol. The next greatest effect was seen for layers formed from acetonitrile solution. The B field reduction was least marked for SAM films formed from toluene and hexane.

We have noted during our experimental programme that voltammograms for ferrocene alkane thiol SAM films are rarely, if ever, ideal in that small but finite anodic/cathodic peak separations ΔE_P

are observed. According to the classic Laviron analysis [13] ΔE_P should be zero for a surface immobilized redox couple. Finklea [2] has noted that non zero peak separations can arise on account of the solvation state of the immobilized redox centers changing with the extent of oxidation of the redox active layer.

Hence strong ion pairs may form in the more highly charged oxidation state and the hydrophilicity/hydrophobicity of the immobilized redox active site may vary as a function of oxidation state. The structure of the SAM film may also change with changes in the degree of oxidation.

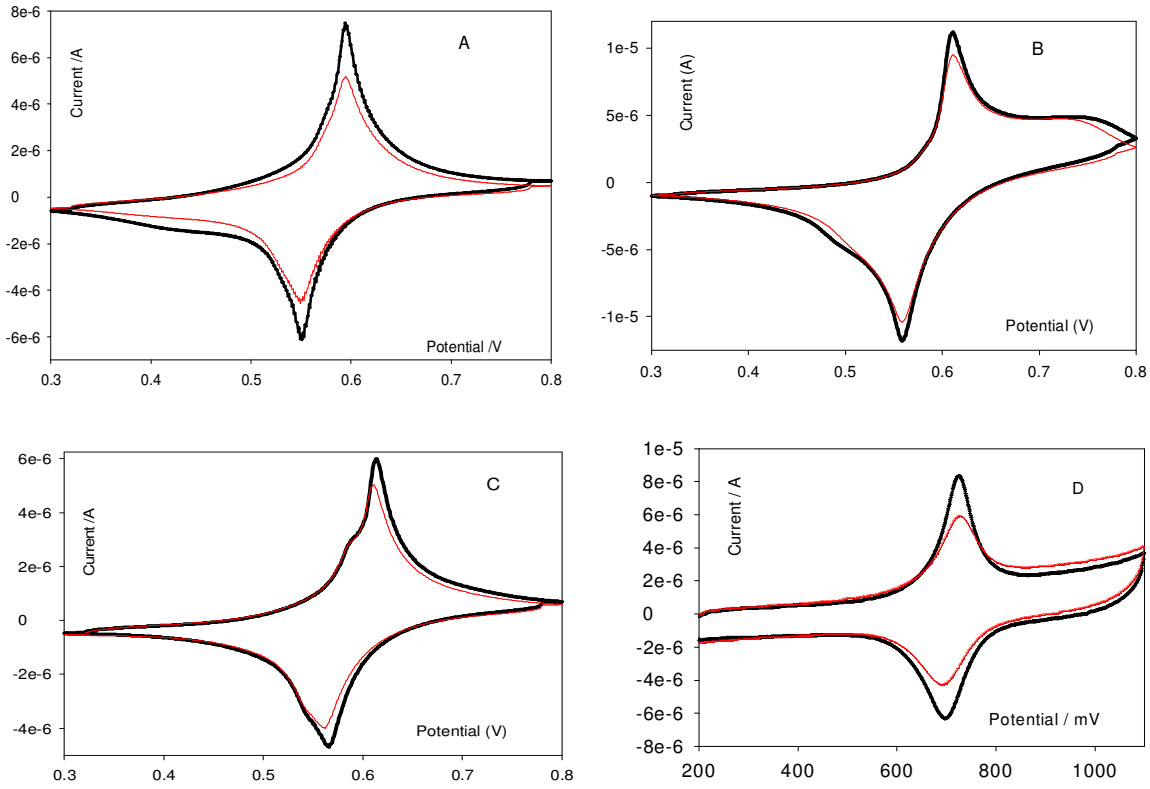

Figure 6. Cyclic voltammograms of a $SH(CH_2)_{10}CO_2Fc$ modified electrodes deposited from 1mM solutions in various solvents. (A) acetonitrile, (B) hexane, (C) toluene and (D) ethanol before (black line) and after (red line) the application of a 0.5T B-field parallel to the surface of the electrode.

Typically peak splitting values are in the range 30-50 mV both in the absence and in the presence of an external magnetic field. In ethanol ΔE_P increases from 29 mV when B = 0 to 33 mV when B = 0.5 T, whereas ΔE_P varies very little in acetonitrile (45 mV vs 44 mV) and toluene (48 mV vs 49 mV) and increases slightly from 52 to 54 mV in hexane.

3.2. Quantifying the effect of external magnetic field on the redox kinetics of monolayer immobilized ferrocene/ferricinium

We now discuss the effects of external magnetic field on the kinetics of the ferrocene/ferricinium surface redox transformation. This must be done using a transient electrochemical method such as cyclic voltammetry, or, as we shall shortly note, potential step chronoamperometry.

In fig. 7 we outline the variation of the oxidative and reductive voltammetric peak potentials recorded for a SAM film formed via passive deposition for from $SH(CH_2)_{12}CO_2Fc$ as a function of sweep rate, both in zero and finite magnetic field. If the surface redox transformations (oxidative ferrocene/ferricinium and reductive ferricinium/ferrocene) were Nernstian then the peak potentials should be invariant with sweep rate. It is clear from fig.7(b) that this pertains only when the experimental timescale is long at low sweep rates. The peak potentials increase significantly with increasing sweep rate when the latter exceeds ca. 10 mVs^{-1}, thus signifying, according to the Laviron analysis [13], that the surface redox transformation is quasireversible. The general trend in peak potential variation is the same independent of magnetic field.

Finklea [2] has noted that immobilized SAM films with pendant ferrocene groups tend to exhibit significantly more positive formal potentials than their solution analogs. The latter shift suggests that the solvation environment of the ferrocene has a lower dielectric constant than the homogeneous solution. Consequently one may infer that the ferrocene group may exhibit a tendency to bury itself in the SAM. Furthermore the presence of electron withdrawing substituents such as CO, COO or CONH attached to the cyclopentadienyl ring can cause a further positive shift in redox peak potential [19]. Hence it is no surprise that the ferrocene/ferrocinium redox chemistry occurs at reasonably elevated potentials as illustrated in fig.7.

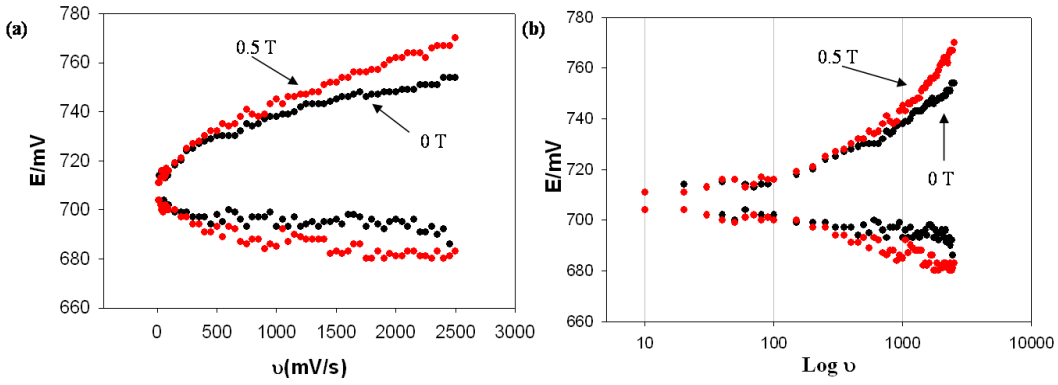

Figure 7. (a) Variation of oxidation and reduction voltammetric peak potentials recorded for ferrocenethiol SAM film formed via passive deposition from 1mM ethanolic solution of $SH(CH_2)_{12}CO_2Fc$ for 49 hours. The CV experiment was performed in 0.1 M $HClO_4$ and the response recorded as a function of sweep rate in the absence (black circle) and in the presence (red circle) of a static 0.5 T magnetic field. (b) Variation of voltammetric peak potentials with logarithm of potential sweep rate recorded under similar conditions to those in fig.7(a).

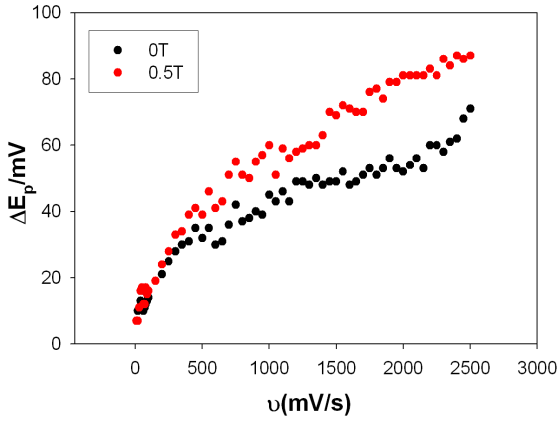

Figure 8. Variation of voltammetric peak separation ΔE_P with sweep rate recorded for the ferrocenethiol SAM film formed via passive deposition from 1mM ethanolic solution of $SH(CH_2)_{12}CO_2Fc$ for 49 hours.

The variation in voltammetric peak separation ΔE_P with experimental time scale expressed as potential sweep rate is illustrated in figure 8. The data was recorded both in zero field conditions and in an external magnetic field of 0.5 T. We immediately note that ΔE_P is non zero and increases regularly with increasing sweep rate both under zero and finite magnetic field conditions. The peak separation recorded in the presence of a magnetic field is slightly larger at a given sweep rate than that recorded under zero field conditions. However peak separations are less than 100 mV even at the largest sweep rates examined (2500 mV/s).

This observation signifies that the redox behaviour is non-ideal and one may well suggest that a well defined potential difference may exist between the support electrode and the site of electron transfer (the surface attached ferrocene moeity). Such a difference could be attributed to the hydrocarbon spacer and the fact that some pendant redox groups may well be buried within the latter material. Furthermore it is clear from fig.7 that the dynamics of the surface redox reaction depends on the experimental time scale (as evidenced by the sweep rate) . This may suggest non ideality in the form of kinetic dispersion effects as we have recently discussed for glucose oxidaser redox chemistry when the latter molecules are immobilized on arrays of single walled carbon nanotubes [20].

It is possible to utilize the well established theory developed by Laviron [13a] to evaluate the electron transfer rate constant from data of the type outlined in figure 7. This can be best accomplished using the methodology outlined in our recent publication [20] where we stated that a linear relationship exists between ΔE_P and natural logarithm of sweep rate:

$$\Delta E_p = \frac{RT}{(1-\beta)\beta F}[\beta \ln(1-\beta) + (1-\beta)\ln\beta - \ln\frac{RT}{F} - \ln k_{ET}{}^0] + \frac{RT}{(1-\beta)\beta F}\ln\upsilon. \qquad (3)$$

The data presented in fig.8 were analysed in terms of eqn.3 and the result illustrated in fig.9. Here linear plots were obtained with well defined slopes and intercepts.

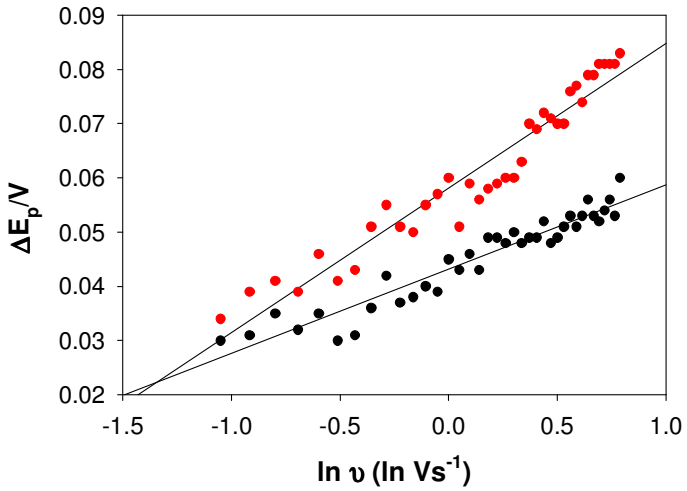

Figure 9. Laviron type plot of voltammetric peak separation variation with logarithm of sweep rate according to expression presented in eqn.3 of text.

Now if S denotes the slope of the Lavron equation plot of the type outlined in fig.9 then from eqn.3 we note that $S = RT/\beta(1-\beta)F = \frac{f}{\beta(1-\beta)}$ where $f = RT/F$. Hence this expression reduces to a quadratic in the parameter β of the form $\beta^2 S - \beta S + f = 0$ which admits the solution: $\beta \cong \frac{1-\sqrt{1-\frac{4f}{S}}}{2}$. Typically for a physically meaningful value of the symmetry factor β which should be close to 0.5, then we note that $4f/S << 1$. Now at 298 K $f \cong 25.7\, mV$. The slope of the graph presented in fig.9 was found to be 15.5 mV for the zero field measurement and 26.7 mV for the experiment performed finite field. Hence the condition $4f/S << 1$ is not satisfied in this situation and we have to resort to another method of data analysis to obtain kinetic information. Similar results were obtained for the other ferrocene alkane thiol SAM films examined, and in all cases ΔE_P was certainly less than 100 mV.

As a result, the Laviron approach [13], which is valid only when $\Delta E_p > 200/n$ mV, is not recommended as a data analysis methodology for this system. Instead we suggest the use of potential step chronoamperometry to calculate rate constants. We have come to a similar conclusion recently when the analysis of surface immobilized flavin redox electrochemistry was examined [20].

In the PS chronoamperometric experiment performed at the SAM/solution interface the potential was stepped from an initial value of ca. 0.30 V to a final value some 550 mV more positive. In effect the potential is stepped across the redox peak, and an oxidative redox transformation ferrocene → ferricinium is established. The current flow arising from the latter is subsequently measured as a function of time. The results of a typical series of oxidative potential step experiments performed on a number of ferrocenyl alkanethiol SAM films in aqueous 0.1 M $HClO_4$ solution are presented in figure 10.

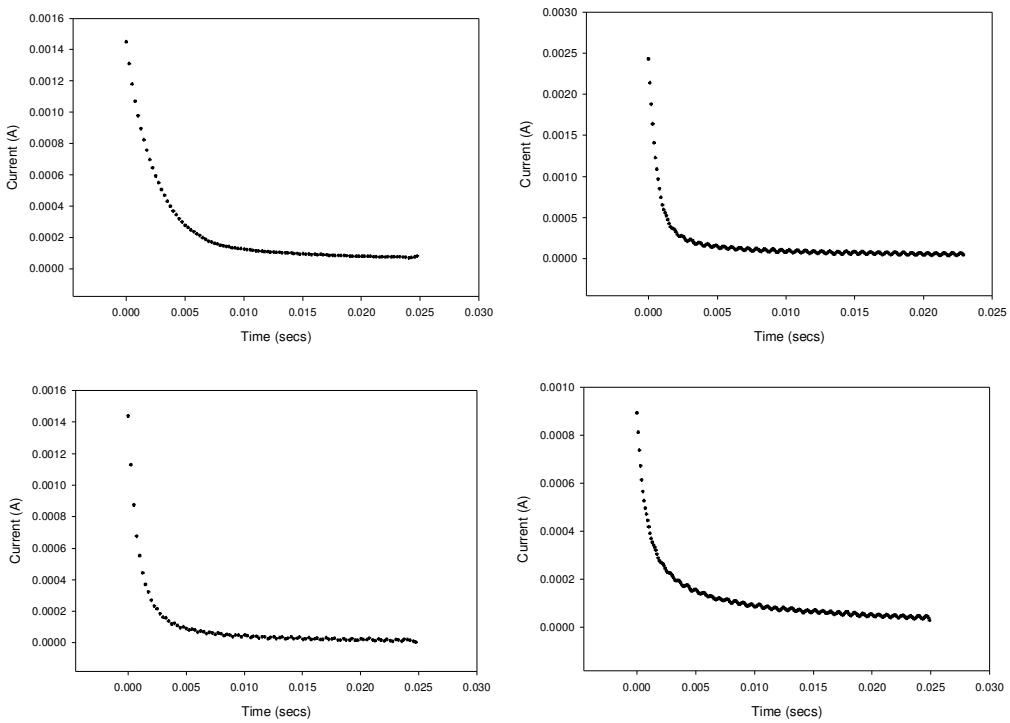

Figure 10. Chronoamperometric response to a potential step over the oxidation peak of the alkanethiol SAM $S(CH_2)_nFcCO_2$ (n=6,8,10,l2). (a) n=6, (b) n=8, (c) n=10, (d) n=12 in 0.1 M $HClO_4$. External magnetic field is absent in this case.

The time varying, chronoamperometric response expected by a surface immobilized redox group arising from a potential step is given by [21]:

$$i = k_{ET}\Delta Q \exp\left[-k_{ET}t\right] \qquad (4)$$

where k_{ET} denotes the potential dependent electron transfer rate constant and ΔQ represents the charge passed during the current transient. We infer from the latter expression that the ferrocene/ferricinium surface redox transformation should exhibit first order kinetics, and consequently, a plot of the natural logarithm of the current should vary linearly with the elapsed time. The slope of the latter plot should then generate a value for the electron transfer rate constant k_{ET}. Typical results obtained for a Ferrocenylcarbonyloxy-decanethiol SAM film are outlined in fig.11(a). It is immediately clear that simple first order kinetics do not pertain since a plot of log current versus time is non-linear. Indeed the semilogarithmic plots exhibit a distinct 'dog-leg' character consisting of two distinct temporal regions. This observation leads to the suggestion that the chronoamperometric response is best expressed in terms of a multiexponential expression where to a first approximation one can indentify a fast and a slow ET

process. The idea is outlined in fig.11(b) where the chronoamperometric response recorded for the C_{10} ferrocenyl alkane thiol SAM is presented.

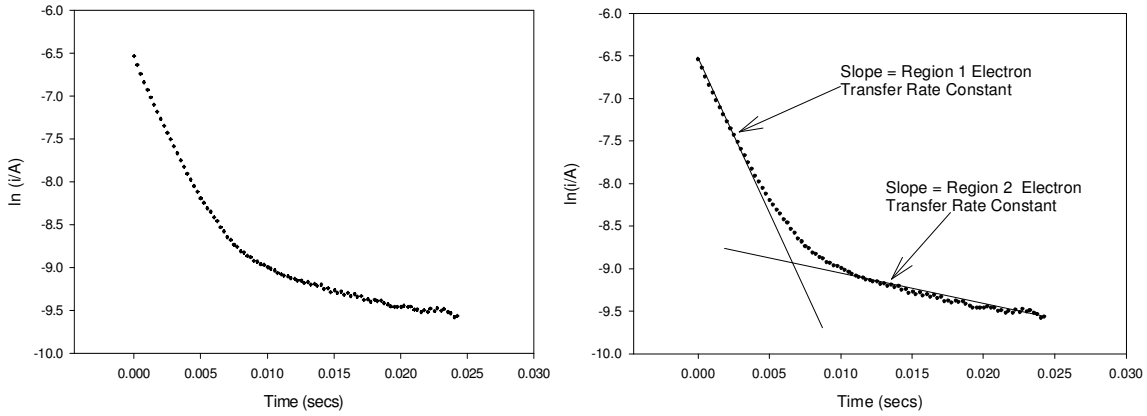

(a) (b)

Figure 11. (a) Semilogarithmic plot of current versus time recorded as a response to a potential step across the oxidation redox peak, for a Ferrocenylcarbonyloxy-decanethiol SAM film in 0.1 M $HClO_4$. (b) Bi-exponential analysis of a typical potential step chronoamperometric plot recorded for the $SH(CH_2)_{12}CO_2Fc$ SAM film in contact with 0.1 M $HClO_4$ solution. The fast and slow kinetic regions are outlined.

Table 1. The electron transfer rate constants extracted from the oxidative chronoamperometry response of an $FcCO_2H(CH_2)_nSH$ (n=6,8,10,12) monolayer.

Electron Transfer Rate Constant (s^{-1})			
n	Chain Length (Å)	$k_{ET,f}$ Region 1	$k_{ET,s}$ Region 2
6	10.2	1024	51
8	12.7	838	82
10	15.2	577	62
12	17.7	365	42

The chronoamperometric response to a potential step for a system exhibiting bi-exponential kinetics is given by [20]:

$$i(t) = A\exp\left[-k_{ET,s}t\right] + B\exp\left[-k_{Et,f}t\right] \qquad (5)$$

Where A,B denote appropriate weighing factors and the substrates s and f refer to slow and fast kinetic processes respectively. It is clear from fig.11(b) that the relaxation time for the fast and slow process is reasonably well separated, and that it is possible to evaluate an expression for the fast and slow rate constants. The results of this type of biexponential analysis for a series of ferrocenyl alkanethiol SAM

films are outlined in table 1. In the latter analysis the chain length (L) is defined as the distance between the carbon linked to the sulfur and the linked carbon of the cyclopentadiene ring. Thus L=0 when the cyclopentadiene carbon is directly linked to the sulfur. Chain lengths are calculated using standard values of CH_2 and ester linker lengths as described by Smalley et al. [22] . It is quite possible that the fast electron transfer rate constant has contains a contribution from double layer charging.

The effect of hydrocarbon chain length on the electron transfer rate constant extracted from the potential step chronoamperometric experiment can be quantified in terms of Marcus theory [2, 23-26]. Using the results shown in Table 1 it is possible to test one of the fundamental predictions of Marcus Theory which governs long range electron transport phenomena which is that the probability of electron transfer depends directly on the distance over which the electron must travel [2]. This is intimately related to the concept of Quantum Mechanical electron tunneling [27,28] and one expects that the electron transfer rate constant should vary with distance according to:

$$k_{ET} = \sqrt{\frac{4\pi^3}{h^2 \lambda RT}} H_{DA}^2 \exp\left[-\frac{\left(\Delta G^0 + \lambda\right)^2}{4\lambda RT} \right] \tag{6}$$

where ΔG^0 and λ denote the thermodynamic driving force for electron transfer and the total re-organization energy for electron transfer respectively. When we consider electron transfer between a surface bound redox group such as ferrocene and the underlying support electrode surface we realise that the process occurs over an extended distance (as illustrated in fig.12) and so the ET process must be non-adiabatic and the extent of electronic coupling between the electrode and the redox group must be weak. The electronic coupling matrix element H_{DA} reflects the strength of interaction between the donor and acceptor states at the transition state and will depend exponentially with distance as follows:

$$H_{DA} = H_{DA}^0 \exp\left[-\beta \left(r - r_0 \right) \right] \tag{7}$$

It is also possible to write for ferrocenyl alkane thiol systems that [28]:

$$k_{ET}(r) = k_{ET}^0 \exp\left[-\beta (r - r_0) \right] = k_{ET}^0 \exp\left[-\beta_n n \right] \tag{8}$$

where β is a parameter related to the probability of electron transfer and measures the sensitivity of the ET reaction rate to distance of the redox group to the underlying electrode surface,and r is the distance over which the electron must travel , effectively the length of the alkane chain. The parameter r_0 is the ET distance corresponding to the idealised Au-S-CO_2Fe$(Cp)_2$ moeity where there are no intervening CH_2 units. We note that the parameter γ is unitless and n denotes the number of repeat methylene units in the hydrocarbon chain, It has been shown that a typical value of β_n for an all trans alkane chain is typically in

the range 0.7-1.1 per CH_2 unit [2, 26(a)]. Hence we expect that a plot of $\log k_{ET}$ vs n should be linear if eqn.8 is valid , and we can evaluate β_n from the slope of the latter plot.

The kinetic data extracted using the bi-exponential analysis [20] illustrated in table 1 is plotted using eqn.8 and the results are presented in fig.13. We note that a good lineaity is observed for the rate constants extracted at short times (region 1 of the chronoamperometric transient) in agreement with eqn.8. In contrast the rate constants evaluated from region 2 at shorter timescales show no such linear trend. It appears that the ET rate constant attains a maximum value for n = 8. Analysis of the linear variation of log k_{ET} with n indicates that $\beta_n \sim 0.17$ which implies that the probability of tunnelling decreases by 0.17 or 17% as each CH_2 unit is added to the hydrocarbon spacer in the SAM film. This value is much lower than that expected for through space electron transfer [21(b,c), 26(a)] and more probably corresponds to a through bond electron transfer. It should be noted however that the k_{ET} values in this region are large and it is difficult to totally deconvolute double layer charging effects from Faradaic electron transfer events at this short timescale.

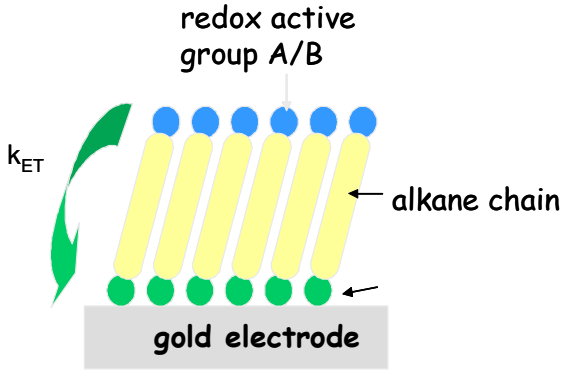

Figure 12. Schematic representation of through bond electron transfer between a tethered redox group and a support electrode surface.

Table 1. The electron transfer rate constants extracted from the oxidative chronoamperometry response of an $FcCO_2H(CH_2)_nSH$ (n=6,8,10,12) monolayer.

Electron Transfer Rate Constant (s^{-1})			
n	Chain Length (Å)	$k_{ET,f}$ Region 1	$k_{ET,s}$ Region 2
6	10.2	1024	51
8	12.7	838	82
10	15.2	577	62
12	17.7	365	42

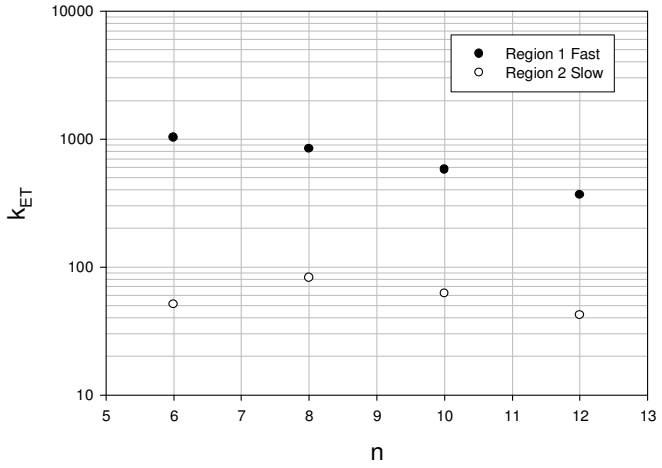

Figure 13. Semi-logarithmic plot of electron transfer rate constant versus number of methylene linkages n for the series of ferrocenyl alkane thiol SAM films in aqueous $HClO_4$ solution.

The fact that the observed rate constants k_{ET} measured at longer timescales do not scale in a semi-logarithmic manner with methylene group number implies that electron transfer may not be the rate determining step at longer times. Indeed as will be discussed in the next section of this paper, the ferrocene/ferricinium redox transformation is accompanied by counter ion transport and ion pair formation and the latter process may prove rate determining in specific circumstances. Typical values for the rate of electron transfer in ferrocenyl based electroactive alkanethiol systems measured using both conventional electrochemical methods and laser induced temperature jump techniques ,lie in the range of $1x10^3$ s^{-1} to $1x10^4$ s^{-1} [9(a),29] and are therefore quite large, and certainly larger than even the fast rate constants measured in this study. Furthermore, the electron transfer rate constants determined in Region 2 are dramatically lower than these expected values. The fact that the rate constants measured in Region 2 for each of the chain lengths are so much lower than these reported values, would indicate that the rate of electron transfer in the system is very much affected by the ability of the pendant ferrocene molecules to form ion pairs with the perchlorate molecules. Thus the formation of ion pairs at the surface of the electroactive SAM is likely to be the rate determining step in the electron transfer. It is quite possible that the smaller values of rate constants extracted from the chronoamperometry data in the present study, and especially those recorded at longer times represent slow ion transport/ion pairing within the SAM layer especially if the redox active ferricinium group is buried within the hydrocarbon matrix in a disordered film. The well cited work of Smalley and co-workers [9(a)] involved the analysis of ferrocenyl alkane thiol monolayers in which the redox active ferrocenes were diluted with non redox active alkane thiols in a controlled manner thereby resulting in a reasonably ordered monolayer structure. Under such circumstances we may well expect to obtain a far larger value for the ET rate constant. Sumner and Creager [30] have suggested that electron transfer is sluggish for ferrocene groups buried within the monolayer interior as compared with those pendant ferrocene groups in contact with a polar solvent. Specifically their experiments indicated that the standard electron transfer rate constant for ferrocene oxidation/reduction in a monolayer of ferrocenyl

decanethiol coadsorbed with decanethiol was typically 4 x 10^4 s^{-1}, whereas that for a monolayer of ferrocenyl decanethiol coadsorbed with 1-mercapto-eicoscane ($C_{20}H_{41}SH$) was ca. 200 s^{-1}. Furthermore the difference in kinetic activity corresponding to buried and exposed ferrocene moieties in the SAM film was found to depend greatly on the size of the electrolyte anion. The ET kinetics was noticibly inhibited when the anion size was large. Again this strongly suggests that electron transfer from the ferrocene unit to the underlying support electrode occurs concomitantly with anion transfer from the electrolyte to the oxidized ferricinium site in the monolayer and the rate of electron transfer can depend critically upon the rate of ion transfer into the monolayer. Such coupled electron/ion transfer is often found when redox switching processes in redox and conducting polymer films are examined [31]. The kinetic analysis of coupled electron and ion transfer has been recently described by Marcus [32] and Saveant [33].

It is also possible to perform this experiment within the bore of a Hallbach magnet in which the magnetic field is set at a value of 0.5 T directed parallel to the plane of the inlaid disc surface. The results obtained in such an experiment at a SAM modified electrode formed via passive deposition from 1mM ethanolic solution of Ferrocenylcarbonyloxy-dodecanethiol $SH(CH_2)_{12}CO_2Fc$ for 49 hours, under both zero and 0.5 T magnetic field conditions, are outlined in semi-logarithmic form in fig 14 below. Again the semi-logarithmic chronoamperometric transients exhibit deviations from simple first order kinetic behaviour..

We can readily note that the semi-logarithmic curve corresponding to the oxidative ferrocene/ferricinium redox transformation decays more rapidly in the presence of an 0.5 T magnetic field than in the field free situation. The heterogeneous rate constant recorded for the ferrocene/ferricinium redox transformation involving electron transfer across the alkane thiol monolayer to an underlying gold electrode was found to be *ca*. 17 s^{-1} when B = 0 T but was significantly increased to *ca*. 47 s^{-1} when B = 0.5 T. In contrast, little effect of magnetic field could be found on the rate constant (k_{ET} = 47 s^{-1} for B = 0 and B = 0.5 T) for the corresponding reductive ferricinium/ferrocene transformation (not shown here), This result provides a firm confirmation for the first time that the rate of long range electron transfer across molecular barriers (the insulating hydrocarbon chains) is directly effected by the presence of a magnetic field. It is significant that the semi-logarithmic plots presented in fig.11 and 14 are not strictly simple first order monoexponential decays. This can be attributed to kinetic dispersion effects [20,34]. Typically when heterogeneous systems such as hydrated oxide thin films, fluorescence decay in membranes, or semiconductor nanoparticle dispersions are subjected to a kinetic analysis, curved semi-logarithmic plots are often observed (as presented in figure 11 and fig.14) when the data is tested for first order kinetics. Albery and co-workers [34] have proposed that it is possible to present an alternative model for kinetics in these dispersed systems. In this approach one assumes a Gaussian distribution in the free energy of activation for the kinetic process and consequently in the logarithm of the rate constant about some mean value. In short a log-normal distribution is assumed [35]. Hence one single adjustable parameter is only introduced- the width γ of the distribution. When $\gamma = 0$ there is no dispersion and the system behaves in a classical homogeneous fashion and first order kinetics are observed. We will not pursue this analysis further here and will revert to it in a future paper. It should also be noted that non linear semilogarithmic chronoamperometry response transients can also arise because of interfacial potential

drop effects across the SAM/electrolyte solution interface [36] as noted by Creager and Weber [37]. This further complicates an already complex situation [38].

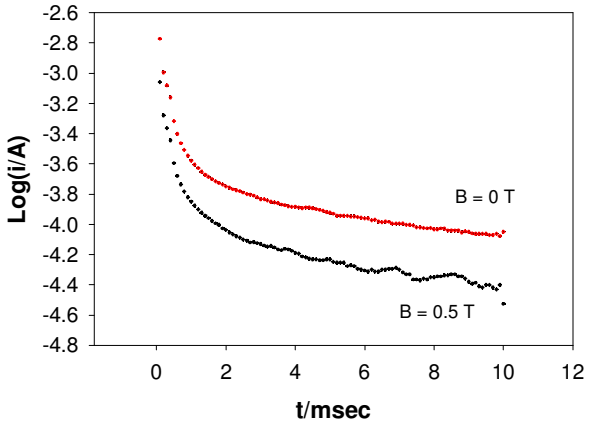

Figure 14. Potential Step chronoamperometric transients recorded in semi-logarithmic format for surface bound Ferrocene/ferricinium redox transition in the absence and presence of an external magnetic field. Potential step 300 – 850 mV. 0.1 M $HClO_4$.

The assertion that kinetic dispersion is important in this system may also be ascertained from cyclic voltammetry experiments conducted as a function of sweep rate. In fig.15 we present the variation of redox group surface coverage Γ recorded for a ferrocene alkane thiol SAM film as a function of applied potential sweep rate or experimental timescale. In this experiment the surface coverage measured at any particular sweep rate reflects the quantity of immobilized ferrocene sites electrochemically addressed and transformed to ferricinium during the time taken for an oxidative sweep. It is clear that the surface coverage decreases progressively with increasing sweep rate regardless of whether an external magnetic field in present. Furthermore, for all values of sweep rate less than a threshold of ca. 2000 mV/s, the surface coverage recorded from voltammograms recorded in a B field of 0.5 T is less than the corresponding value recorded under zero field conditions. For sweep rates greater than 2000 mV/s no difference in surface coverage is determined for measurements conducted in zero and finite B field. The difference between zero and finite B field coverage is greatest for the lowest sweep rates, i.e. for longest experimental time scales. Similar behaviour was observed for other ferrocene alkane thiol SAM films as illustrated in figure 14. We note for the latter films (C_{10} and C_8 ferrocenyl alkane thiols) that the coverage drops very quickly in the sweep rate region between 1 and 100 mV/s and only slowly thereafter regardless of whether a magnetic field is present.

These voltammetric results can be rationalized if we assume that there exists a distribution (perhaps Gaussian) of electron transfer distances in the immobilized redox active SAM layer. In essence some ferrocene groups are located closer to the support electrode surface than others and therefore will have larger ET rate constants since the electron transmission probability for through bond electron transfer will be larger. Hence the surface coverage is largest when determined by integrating voltammograms at the longest time scale (the smallest sweep rate) since most if not all tethered ferrocene

sites can then react during the timescale involved. Conversely far fewer ferrocene sites can react at faster timescales and the surface coverage determined under such conditions is correspondingly lower.

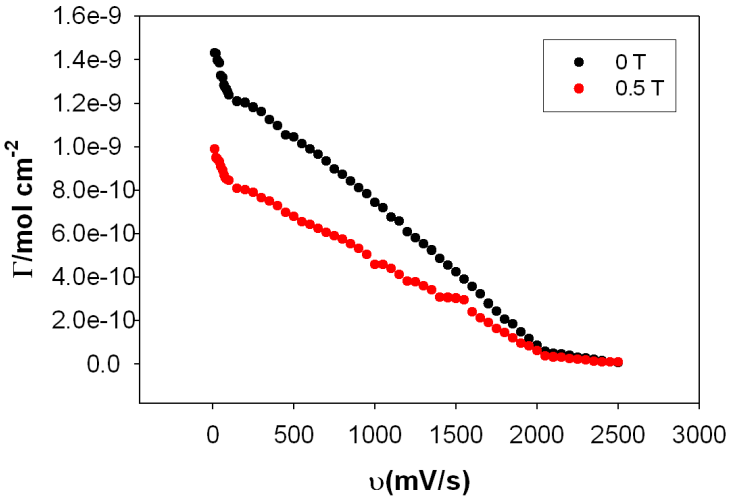

Figure 15. Variation of surface coverage with sweep rate for a ferrocene alkane thiol SAM modified electrode formed via passive deposition from 1mM ethanolic solution of $SH(CH_2)_{12}CO_2Fc$ for 49 hours. The voltammetry was performed in 1M $HClO_4$ both in the absence and in the presence of an external magnetic field (B = 0.5 T).

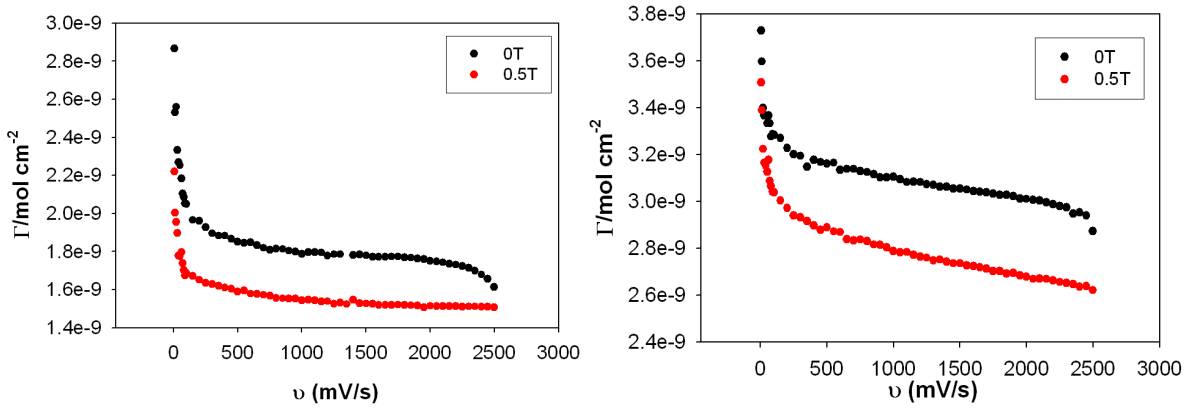

Figure 16. Variation of integrated surface coverage with potential sweep rate for (a) C_{10} ferrocenyl alkane thiol and (b) C_8 ferrocenyl alkane thiol SAM films in 1.0 M $HClO_4$. The experiments were performed both in zero and finite magnetic field environments.

Sumner and Creager [30] have suggested that through bond electron transfer is more sluggish for ferrocene groups buried within the monolayer interior compared with those ferrocene groups in direct contact with a polar electrolyte medium. Also they suggested that the ferrocene/ferricinium reaction must be considered as a coupled electron transfer/ion transfer process : electron transfer rate depends crucially on electrolyte anion size. Large anions diffuse slowly in the SAM and the net rate of redox

transformation in the monolayer may well depend on the rate of counterion diffusion to the oxidized ferricinium moeity to form a contact ion pair. We again suggest that a considerable fraction of ferrocene sites may be buried within the SAM and that ion ingress to the latter during oxidation may be inhibited thereby slowing down thevoltammetric response and thereby resulting in a decrease in the quantity of ferrocene sites electrically addressed as manifested in the measured value of the surface coverage. decreasing the observed electron transfer rate constant.

To further elucidate the redox switching dynamics at the SAM/solution interface an electrochemical quartz crystal microbalance (EQCM) was employed to directly investigate the mass changes at the monolayer/solution interface during redox switching. The results obtained for a variety of ferrocenyl alkane thiol SAM modified electrodes using an electrochemical cell specifically designed for EQCM work are presented in fig. 17 below.

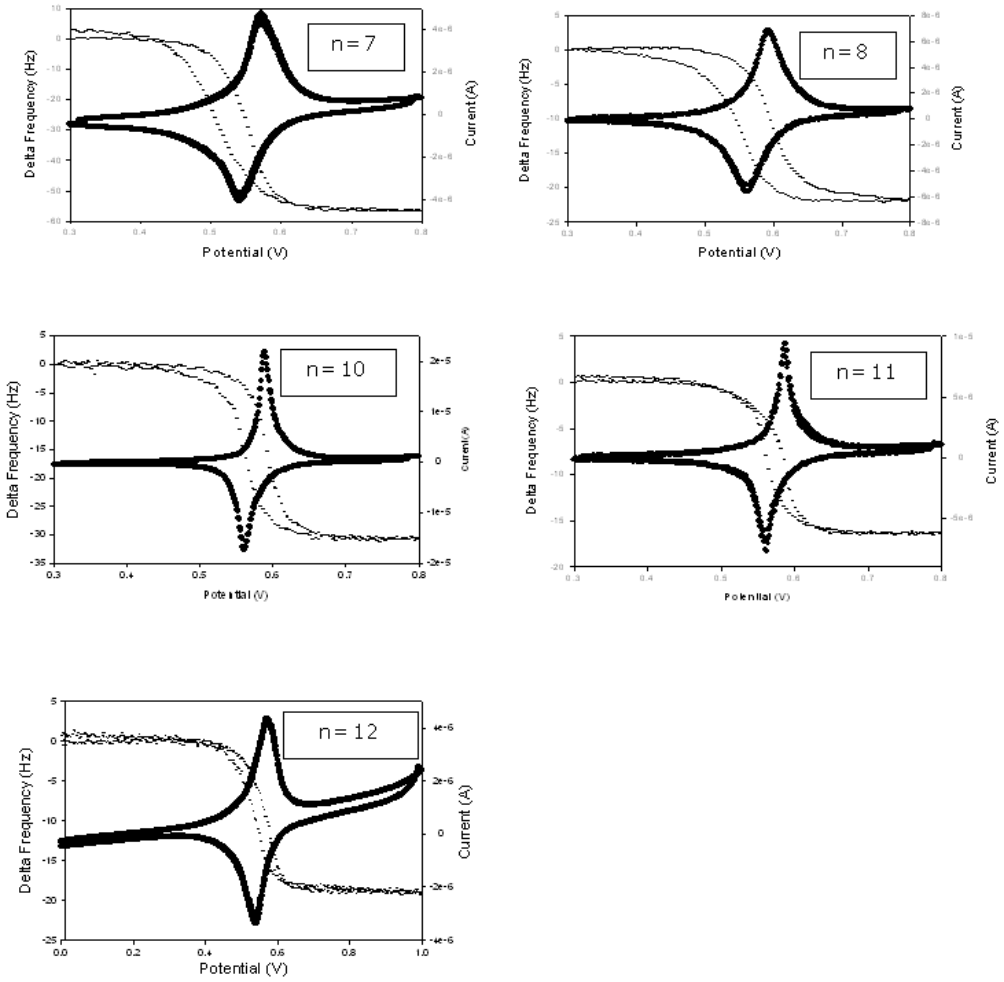

Figure 17. CV (dark trace) and frequency change (light trace) corresponding to the oxidation of $S(CH_2)_nCO_2HFc$(n=7,8,10,11,12) SAM modified Au electrodes in 0.1 M $HClO_4$.

Oxidation of the surface immobalized ferrocene group to ferricinium is clearly accompanied by a significant decrease in oscillation frequenncy indicating an increase in the total mass of the SAM film. This can be attributed to the formation of an ion pair between the positively charged ferricinium group and a perchlorate ion. The redox process in this case is expressed as follows,

$$Fc \rightarrow Fc^{+} + e^{-}$$

$$Fc^{+} + X^{-} \rightarrow Fc^{+}X^{-}$$

where $Fc^{+}X^{-}$ represent the ion pair formed and $X^{-} = ClO_4^{-}$. The EQCM frequency changes recorded over the redox switching region and the corresponding mass change (derived from the Sauerbrey Equation [11]) are presented in table 2 below for all ferrocenyl alkane thiol films examined. Now the average surface coverage for the ferrocenyl alkane thiol SAM films presented in fig.17 is 3.3 x 10^{-10} mol cm^{-2} which is, within experimental error close to the theoretical limit of 4.5 x 10^{-10} mol cm^{-2} calculated by Chidsey [18] assuming a close packed layer of 6.6 angstroms diameter spheres. Hence the average mass increase is Δm = 29 ng. From the average surface coverage value we can determine the number of adsorbed ferrocent molecules per unit area $N = \Gamma N_A = 1.9\times10^{14}$. The latter number also defined the number of ion pairs assuming all oxidized groups form ion pairs with perchlorate ions from solution. Hence 1.9×10^{14} ClO_4^{-} ions are incorporated into the SAM film during redox switching. Now a single ClO_4^{-} ion has a mass of 99.45 g mol^{-1} or 1.6×10^{-22} g $molecule^{-1}$. Hence the mass change expected for the incorporation of 1.9×10^{14} ClO_4^{-} ions is $\Delta m = 31\, ng$. This value is very close to the average mass change recorded for all the SAMs investigated. Hence we can conclude that, on average, complete charge compensation is achieved from ion pairing at the SAM/solution interface.

Table 2. EQCM frequency changes due to the oxidation of Fc to Fc^{+} and the corresponding formation of an ion pair on the SAM surface. Frequency changes are shown for $S(CH_2)_nCO_2HFc$ where n = 7, 8,10,11, 12.

n	Oxidation Potential range	Frequency Change (Hz)	Mass Change (Δm) (ng)
7	0.45V – 0.65V	19.6	27
8	0.45V – 0.65V	18.2	26
10	0.5V – 0.7V	29.2	42
11	0.5V – 0.7V	16.6	23
12	0.5V – 0.7V	18.5	26

Inspection of table 2 reveals that the monolayer formed from $S(CH_2)_{10}CO_2Fc$ undergoes a considerably larger mass increase than any of the other chain length thiols. The mass increase can be

attributed to the ingress of solvent molecules as well as charge compensating counterions during the oxidative redox switching process.

This study has shown that ion pairing between oxidised ferrocene molecules and electrolyte counter ions does occur and that a monolayer of anions are present on the surface of the SAM during oxidation. It is also noted that a corresponding decrease in the surface mass of the SAM occurs upon reduction. This corresponds to the ferricenium cation returning to the neutral ferrocene and the ClO_4^- anions returning to solution.

The theory developed some time ago by Smith and White [36a] enables SAM voltammetry to be quantitatively examined. Specifically, the shape of the voltammetric wave and the position at which it is observed to be computed from a simple double layer model and it has been shown that the shape and peak position depend on the thickness and dielectric constant of the adsorbate film, the surface concentration of electroactive adsorbate, the concentration and type of charge compensating solution phase counterion, the solvent dielectric constant and the potential of zero charge. This type of analysis was further developed by Ohtani and co-workers [36b] and by Calvente and co-workers [39]. Hence keeping this work in mind we note that the shape of the voltammetric response recorded for a redox active SAM film such as the systems discussed in the present paper is strongly dependent on the distribution of potential at the monolayer/solution interface [36,37]. The potential distribution in turn is determined by the distribution of charge compensating counterions in the solution adjacent to the monolayer. The voltammetric profile will also be directly effected by the degree of ion pairing and ion association and on whether the immobilized redox groups are buried within the dielectric thiol film. Clearly the counterion distribution will be disturbed by the local stirring effect brought about by the magnetohydrodynamic Lorenz force. This will directly effect the number of local available counterions whih can engage in ion pairing with oxidized ferricinium groups and hence, as Smith and White [36a] have shown quantitatively, effect the nature of the interfacial potential distribution.. Indeed the packing quality and structure of the monolayer film may well suffer irreversible change as a result of this local stirring. This will be reflected in the change in voltammetric response such as that shown in fig.5, fig. 6 and quantitatively in fig. 15 and fig. 16.

4. CONCLUSIONS

In this paper we have examined the redox behaviour of ferrocene alkane thiol self assembled monolayer modified electrodes in contact with aqueous perchlorate solutions both in the absence of and in the presence of an external magnetic field. We have shown that the voltammetric response recorded is irreversibly effected by the imposition of a static magnetic field of magnitude 0.5 T, and that the surface coverage of electroactive ferrocene surface groups and the electrochemical rate constant for the ferrocene/ferricinium surface redox transformation is quantitatively influenced by the imposition of the external magnetic field. We suggest that the latter redox transformation is accompanied by ion pair formation between the ferricinium and perchlorate ions . The magnetic field dependence of the redox behaviour can be attributed to structural changes in the monolayer arising

from double layer effects involving changes in the spatial distribution of perchlorate counterions at the monolayer/solution interface, the latter brought about by local convective stirring arising from the B field generated magnetohydrodynamic Lorenz body force.

ACKNOWLEDGEMENTS.
The authors acknowledge funding from HEA-PTRLI Research Program 'New Chemical Dimensions in Nanomaterials', IRCSET Basic Research Grant SC/02/169 and Enterprise Ireland Basic Research Grant SC/03/49.

References

1. R.L Carroll and C.B. Gorman, B., *Angew. Chem. Int. Ed.,* 41(2002) 4378.
2. H.O. Finklea , *Electroanalytical Chemistry A.J. Bard, I. Rubenstein (Eds)*; Marcel Dekker, New York, 19(1996) 105-335.
3. (a) T.Z. Fahidy, *J. Appl. Electrochem.* 13(1983)553; (b) R.A. Tacken, L.J.J. Janssen, *J. Appl. Electrochem*. 25(1995) 1.
4. (a) R. Aogaki, K. Fueki, and T. Mukaibo, *Denki Kagaku*, 43(1975) 504, 509 ; (b) O. Aabouki, J. -P. Chopart, J. Douglade, A. Olivier, C. Gabrielli, and B. Tribollet, *J. Electrochem. Soc.* 137(1990) 1796; (c) G. Hinds, J.M.D. Coey, and M.E.G. Lyons, *Electrochem. Commun.* 3(2001) 215; (d) G. Hinds, F.E. Spada, J.M.D. Coey, T.R. Ni Mhiochain, and M.E.G. Lyons, *J.Phys. Chem.B.* 105(2001) 9487; (e) O. Aaboubi, P. Los, J. Ambiard, J.-P. Chopart, and A. Olivier, *J. Electrochem. Soc.* 150(2002) E125.
5. (a) J.C.Shannon, Z.H. Gu and T.Z. Fahidy, *J.Electrochem Soc.* 144(1997) L314 ; (b) I. Mogi and M.Kamiko, *J. Crystal Growth*, 166(1996) 276 ; (c) O. Devos, A. Olivier, J.P. Chopart, O. Aaboubi and G. Maurin, *J. Electrochem. Soc.* 145(1998) 401 ; (d) C.O'Reilly, G. Hinds and J.M.D. Coey, *J. Electrochem. Soc.* 148(2001) C674.
6. O.Devos, O. Aaboubi, J.-P. Chopart, A. Olivier, C. Gabrielli, and B. Tribollet , *J. Phys. Chem. A*. 104(2000) 1544.
7. C.-C. Lee and T.-C. Chou, *Electrochim. Acta*. 40(1995) 965.
8. C. MacGloinn, M.Sc. Thesis, School of Chemistry, University of Dublin, Trinity College, 2006.
9. (a) J.F. Smalley, S.W. Feldberg, C.E.D. Chidsey, M.R. Linford, M.D. Newton and Y.P. Liu, J. Phys. Chem. B., 99(1995) 13141. (b) R.O'Brien, Characterisation of n-ferrocenyl alkanethiol self-assembled monolayers. Ph.D Thesis, School of Chemistry,University of Dublin, 2007. (c) A.M. Napper, H. Lui and D.H. Waldeck, *J. Phys. Chem. B.* 105(2001) 7699.
10. P.C. Reeves, *Organic Syntheses*, 6(2002) 625.
11. G. Sauerbrey, Z. Phys., 155(1959)206.
12. P. Brown, M.Sc Thesis, Characterization and shimming of magnetic field profiles produced by Hallbach cylinders. School of Physics, University of Dublin, Trinity College, 1996.
13. (a) E. Laviron, *J. Electroanal. Chem.* 100(1979) 263; (b) E. Laviron, *J. Electroanal. Chem.* 101(1979) 19; (c) E. Figgemeier, L. Mertz, B.A. Hermann, Y.C. Zimmermann, C.E. Houscroft, H.-J. Guntherodt, and E.C. Constable, *J. Phys. Chem.B*. 107(2003) 1157.
14. D.D. Popnoe, R.S. Deinhammer, M.D. Porter, *Langmuir*, 8(1992) 2521.
15. R.Prins, A.R. Korswagen, A.G.T.G.Kortbeek, *J. Organomet. Chem*., 39(1972)335.
16. J.Holecek, K. Handlir, J. Klikorka, N. Dinh Bang, *Collect. Czech Chem. Commun.*, 44(1979) 1379.
17. M. Kinsella, *Ph.D Thesis,* School of Chemistry, University of Dublin, Trinity College, 2006.
18. C. E. D Chidsey. *Science,*251(1991) 919.
19. T. Kondo, M. Takechi, Y. Sato, K. Uosaki, *J. Electroanal. Chem.* 381(1995) 203.
20. M.E.G. Lyons and G.P. Keeley, *Int. J. Electrochemical Science*, 3 (2008) 819.

21. (a) M.E.G. Lyons, *Sensors*, 2 (2002) 314. (b) R.J. Forster, L.R. Faulkner, *J. Am. Chem. Soc.,* 116 (1994) 5444. (c) R.J. Forster, L.R. Faulkner, *J. Am. Chem. Soc.,* 116(1994) 5453. (d) H.O. Finklea, D.D. Hanshew, *J. Am. Chem. Soc*., 114 (1992) 3173. (e) V. kertesz, J.Q. Chambers, A.N. Mullenix, *Anal. Chem.*, 71 (1999) 3905.
22. J. F. Smalley, H. O. Finklea, C. E. D. Chidsey, M. R. Linford, S. E. Creager, J. P. Ferraris, K. Chalfant, T. Zawodzinsk, S. W. Feldberg, and M. D. Newton, *J. Am. Chem. Soc.* 125(2003) 2004.
23. The literature is this area is vast. The following can be recommended although the list is not exhaustive. (a) R.A. Marcus, *J. Electroanal. Chem*., 438(1997) 251 (Nobel Lecture). (b) R.A. Marcus and N. Sutin, *Biochimica et Biophysica Acta*, 811(1985) 265. (c) L.J.C. Jeuken, *Biochimica et Biophysica Acta,* 1604(2003) 67. (d) H.B. Gray, J.R. Winkler, *Annu. Rev. Biochem*., 65(1996) 537.(e) E.S. Medvedev, A.A. Stuchebrukhov, *Pure & Appl. Chem*., 79(1998) 2201. (f) D.M. Adams et al. *J. Phys. Chem.B.,* 107(2003) 6668.
24. (a) P.F. Barbara, T.J. Meyer, M.A. Ratner, *J. Phys. Chem*., 100(1996) 13148. (b) S. Berchmans, R.G. Nirmal, G. Prabahran, A.K. Mishra, V. Yegnaraman, *J. Solid State Electrochem*., 10(2006) 439. (c) N. Sutin, B.S. Brunschwig, C. Creutz, S.W. Feldberg, *J. Phys. Chem.B.,* 108(2004) 12092. (d) N. Sutin, B.S. Brunschwig, C. Creutz, *J. Phys. Chem.,B.,* 107(2003) 10687. (e) A.C. Benniston, A. Harriman, *Chem. Soc. Rev*., 35(2006) 169. (f) M.D. Newton, J.F. Smalley, *Phys. Chem. Chem. Phys.*, 9(2007) 555.
25. M.D. Newton, N. Sutin, *Ann. Rev. Phys. Chem.*, 35(1984) 437. (b) N. Sutin, *Acc. Chem. Res*.,15(1982) 275. (c) M.D. Newton, *Chem. Rev*. 91 (1991) 767. (d) M.T. Carter, G.K. Rowe, J.S. Richardson, L.M. Tender, R.H. Terrill, R.W. Murray, *J. Am. Chem. Soc*., 117 (1995) 2896. (e) K. Weber, L. Hockett, S. Creager, *J. Phys. Chem. B.*, 101 (1997)8286. (f) S.P. Dudek, H.D. Sykes, C.E.D. Chidsey, *J. Am. Chem. Soc.,* 123 (2001) 8033. (g) L.A. Hockett, S.E. Creager, *Langmuir,* 11 (1995) 2318. (h) J.N. Richardson, S.P. Peck, L.S. Curtin, L.M. Tender, R.H. Terrill, M.T. Carter, R.W. Murray, G.K. Rowe, S.E. Creager, *J. Phys. Chem*., 99 (1995) 766. (i) J.F. Smalley, S.W. Feldberg, C.E.D. Chidsey, M.R. Linford, M.D. Newton, Y-P. Liu, *J. Phys. Chem*., 99(1995) 13141.
26. D.N. Beratan, J.J. Hopfield, *J. Am. Chem. Soc.*, 106(1984) 1584. (b) C. Liang, M.D. Newton, *J. Phys. Chem.*, 96 (1992) 2855. (b) C. Liang, M.D. Newton, *J. Phys. Chem*., 97 (1993) 3199. (c) D.N. Beratan, J.N. Betts, J.N. Onuchic, *J. Phys, Chem*., 96 (1992) 2852. (d) J. Malinsky, Y. Magarshak, J. Phys. Chem., 96 (1992) 2849. (e) C. Miller, M. Gratzel, *J. Phys. Chem*. 95 (1991) 5225. (f) S.W. Feldberg, M.D. Newton, J.F. Smalley, *Electroanal. Chem.,* A.J. Bard, I. Rubenstein (Eds), 22 (1994) 102-181. (g) A.M. Kuznetsov, J. Ulstrup, *J. Incl. Phenomen. & Macrocyc. Chem.,* 35(1999) 45.
27. J.O.M. Bockris and S.U.M. Khan, *Quantum Electrochemistry*, Plenum Press, New York, 1979, Chapter 8, pp.235-289. (b) C.J. Miller, *Physical Electrochemistry* (I. Rubenstein (Ed)), Chapter 2, pp.27-79, Dekker, New York, 1995.
28. M.T. Carter, G.K. Rowe, J.N. Richardson, L.M. Tender, R.H. Terrill, R.W. Murray, J. Am. Chem. Soc., 117 (1995) 2896.
29. J.J. Sumner, K. S. Weber, L.A. Hockett, S.E. Creager, *J. Phys. Chem. B*., 204 (2000) 7449.
30. J.J. Sumner, S.E. Creager, *J. Phys. Chem.B.,* 105 (2001) 8739.
31. M.E.G. Lyons in *Electroactive Polymer Electrochemistry*, (M.E.G. Lyons (Ed)), Plenum Press, New York, 1994, Chapter 1, pp.1-235.
32. R.A. Marcus *J. Phys. Chem.B.*, 102 (1998) 10071.
33. J.M. Saveant, *J. Phys. Chem.B.*, 105 (2001) 8995.
34. W.J. Albery, P.N. Bartlett, C.P. Wilde, J.R. Darwent, *J. Am. Chem. Soc.,* 107 (1985) 1854.
35. See for example the excellent Wikipedia definition at http://en.wikipedia.org/wiki/Log-normal_distribution.
36. (a) C.P. Smith, H.S. White, *Anal. Chem.,* 64 (1992) 2398. (b) M. Ohtani, S. Kuwabata, H. Yoneyama, *Anal. Chem.*, 69 (1997) 1045.

37. S.E. Creager, K. Weber, *Langmuir*, 9(1993) 844.
38. L.J.C. Jeuken, *Biochimica et Biophysica Acta*, 1604(2003) 6
39. J.J. Calvente, R. Andreu, M. Molero, German Lopez-Perez, M. Dominguez, *J. Phys. Chem.B.,* 105 (201) 9557.